Electronic supplementary information

What determines the Th/U atom positions inside fullerenes?

Jilong Chen, Lei Lou and Peng Jin*

School of Materials Science and Engineering, Hebei University of Technology, Tianjin 300401, China. E-mail: china.peng.jin@gmail.com

Table S1 Summary of electronic ground state, metal valence state, metal position and the nearest metal-cage distances (M-C; Å) of all actinide mono-EMFs obtained by using different experimental/theoretical methods. The major metal site from single-crystal X-ray diffraction (XRD) is given if disordered.

Species	Method	Ground state	Metal valence	Metal position	M-C	Ref.
Th@T_d(2)-C_{76}	XRD			sumanene	2.39	1
	M06-2X	singlet	+4	sumanene	2.46	2
	B3LYP	singlet	+4	sumanene	2.48	3
	M06-2X	singlet	+4	sumanene	2.47	this work
	PBE0	singlet	+4	sumanene	2.46	this work
	PBE	singlet	+4	sumanene	2.48	this work
Th@C_1(17418)-C_{76}	XRD			PA	2.36	4
	B3LYP	singlet	+4	PA	2.50	3
	M06-2X	singlet	+4	PA	2.46	this work
	PBE0	singlet	+4	PA	2.46	this work
	PBE	singlet	+4	PA	2.49	this work
Th@D_{5h}(6)-C_{80}	XRD			[6,6] bond	2.33	5
	PBE0	singlet	+4	[6,6] bond	2.42	5
	M06-2X	singlet	+4	[6,6] bond	2.39	this work
	PBE0	singlet	+4	[6,6] bond	2.39	this work
	PBE	singlet	+4	[6,6] bond	2.41	this work
Th@C_1(28324)-C_{80}	XRD			PA	2.37	6
	PBE	singlet	+4	PA	2.50	6
	M06-2X	singlet	+4	PA	2.46	this work
	PBE0	singlet	+4	PA	2.46	this work
	PBE	singlet	+4	PA	2.48	this work
Th@C_2(5)-C_{82}	XRD			hexagon	2.31	7
	PBE	singlet	+4	hexagon	2.46	7
	M06-2X	singlet	+4	hexagon	2.43	this work
	PBE0	singlet	+4	hexagon	2.44	this work

	PBE	singlet	+4	hexagon	2.46	this work
Th@C_{3v}(8)-C_{82}	XRD			phenalene	2.34	8
	BP86	singlet	+4	phenalene		8
	BLYP	singlet	+4	phenalene	2.37	9
	M06-2X	singlet	+4	phenalene	2.36	this work
	PBE0	singlet	+4	phenalene	2.36	this work
	PBE	singlet	+4	phenalene	2.38	this work
Th@C_{2v}(9)-C_{82}	XRD			phenalene	2.35	7
	PBE	singlet	+4	phenalene	2.39	7
	M06-2X	singlet	+4	phenalene	2.36	this work
	PBE0	singlet	+4	phenalene	2.36	this work
	PBE	singlet	+4	phenalene	2.38	this work
Th@C_2(8)-C_{84}	XRD			sumanene	2.36	10
	PBE0	singlet	+4	sumanene	2.46	10
	M06-2X	singlet	+4	sumanene	2.43	this work
	PBE0	singlet	+4	sumanene	2.44	this work
	PBE	singlet	+4	sumanene	2.46	this work
Th@C_s(15)-C_{84}	XRD			sumanene	2.27	10
	PBE0	singlet	+4	sumanene	2.46	10
	M06-2X	singlet	+4	sumanene	2.43	this work
	PBE0	singlet	+4	sumanene	2.44	this work
	PBE	singlet	+4	sumanene	2.46	this work
Th@C_1(11)-C_{86}	XRD			sumanene	2.33	11
	BP86	singlet	+4	sumanene	2.49	11
	M06-2X	singlet	+4	sumanene	2.44	this work
	PBE0	singlet	+4	sumanene	2.45	this work
	PBE	singlet	+4	sumanene	2.47	this work
Th@C_2(14)-C_{86}	XRD			sumanene	2.35	12
	PBE0	singlet	+4	sumanene	2.47	12
	M06-2X	singlet	+4	sumanene	2.45	this work
	PBE0	singlet	+4	sumanene	2.45	this work
	PBE	singlet	+4	sumanene	2.47	this work
Th@C_3(18)-C_{86}	XRD			sumanene	2.40	12
	PBE0	singlet	+4	sumanene	2.46	12
	M06-2X	singlet	+4	sumanene	2.43	this work
	PBE0	singlet	+4	sumanene	2.44	this work
	PBE	singlet	+4	sumanene	2.47	this work
U@D_{3h}-C_{74}	XRD			[6,6] bond	2.33	13
	BP86	triplet	+4	[6,6] bond	2.39	13,14
	M06-2X	triplet	+3	[6,6] bond	2.45	this work
	PBE0	triplet	+4	[6,6] bond	2.38	this work

	PBE	triplet	+4	[6,6] bond	2.38	this work
U@C_1(17418)-C_{76}	XRD			PA	2.29	6
	PBE	triplet	+4	PA	2.41	6
	M06-2X	triplet	+3	PA	2.47	this work
	PBE0	triplet	+3	PA	2.44	this work
	PBE	triplet	+4	PA	2.42	this work
U@C_1(28324)-C_{80}	XRD			PA	2.27	6
	PBE	triplet	+4	PA	2.42	6
	BP86	triplet	+4	PA	2.43	14
	M06-2X	triplet	+4	PA	2.39	this work
	PBE0	triplet	+4	PA	2.40	this work
	PBE	triplet	+4	PA	2.42	this work
U@C_s(4)-C_{82}	XRD			sumanene	2.38	15
	PBE	triplet	+4	sumanene	2.40	15
	M06-2X	triplet	+3	sumanene	2.45	this work
	PBE0	triplet	+4	sumanene	2.41	this work
	PBE	triplet	+4	sumanene	2.42	this work
U@C_2(5)-C_{82}	XRD			[5,6] bond	2.24	13
	BP86	triplet	+4	[5,6] bond		13
	M06-2X	triplet	+3	[5,6] bond	2.45	this work
	PBE0	triplet	+3	[5,6] bond	2.42	this work
	PBE	triplet	+4	[5,6] bond	2.43	this work
U@C_s(6)-C_{82}	XRD			phenalene	2.39	16
	M06-2X	triplet	+3	phenalene	2.39	this work
	PBE0	triplet/quintet	+3/+3	phenalene/ phenalene	2.38/2.39	this work
	PBE	triplet	+3	phenalene	2.35	this work
U@C_{2v}(9)-C_{82}	XRD			hexagon	2.41	13
	BP86	triplet	+3	hexagon		13
	BLYP	triplet	+3	hexagon	2.43	9
	M06-2X	triplet	+3	hexagon	2.39	this work
	PBE0	triplet/quintet	+3/+3	hexagon/ hexagon	2.38/2.40	this work
	PBE	triplet	+3	hexagon	2.37	this work
U@C_2(8)-C_{84}	XRD			sumanene	2.28	16
	M06-2X	triplet	+3	sumanene	2.44	this work
	PBE0	triplet	+4	sumanene	2.40	this work
	PBE	triplet	+4	sumanene	2.41	this work
U@C_s(15)-C_{84}	XRD			sumanene	2.32	16
	M06-2X	triplet	+3	sumanene	2.43	this work
	PBE0	triplet	+4	sumanene	2.40	this work

	PBE	triplet	+4	sumanene	2.41	this work
U@D_2(21)-C_{84}	XRD			hexagon	2.20	17
	M06-2X	quintet	+3	hexagon	2.41	this work
	PBE0	triplet/quintet	+3/+3	hexagon/ hexagon	2.40/2.40	this work
	PBE	triplet	+3	hexagon	2.38	this work
U@C_1(11)-C_{86}	XRD			sumanene	2.31	17
	M06-2X	triplet/quintet	+3/+3	sumanene/ sumanene	2.41/2.48	this work
	PBE0	triplet	+4	sumanene	2.41	this work
	PBE	triplet	+4	sumanene	2.42	this work
U@C_1(12)-C_{86}	XRD			sumanene	2.28	16
	M06-2X	triplet	+3	sumanene	2.35	this work
	PBE0	triplet	+3	sumanene	2.43	this work
	PBE	triplet	+4	sumanene	2.42	this work
U@C_s(15)-C_{86}	XRD			hexagon	2.21	17
	M06-2X	triplet	+3	hexagon	2.41	this work
	PBE0	triplet	+3	hexagon	2.40	this work
	PBE	triplet	+4	hexagon	2.38	this work

Table S2 Relative energies (ΔE, kcal/mol) of all actinide mono-EMFs with different spin multiplicities (M) at different theoretical levels.

Species	M	M06-2X	PBE0	PBE
Th@T_d(2)-C_{76}	**1**	**0.0**	**0.0**	**0.0**
	3	17.0	13.0	10.5
Th@C_1(17418)-C_{76}	**1**	**0.0**	**0.0**	**0.0**
	3	20.3	23.9	19.8
Th@D_{5h}(6)-C_{80}	**1**	**0.0**	**0.0**	**0.0**
	3	15.7	12.0	10.4
Th@C_1(28324)-C_{80}	**1**	**0.0**	**0.0**	**0.0**
	3	32.2	27.1	23.2
Th@C_2(5)-C_{82}	**1**	**0.0**	**0.0**	**0.0**
	3	13.9	10.7	9.2
Th@C_{3v}(8)-C_{82}	**1**	**0.0**	**0.0**	**0.0**
	3	12.4	25.7	21.9
Th@C_{2v}(9)-C_{82}	**1**	**0.0**	**0.0**	**0.0**
	3	22.3	18.2	14.7

Th@C_2(8)-C_{84}	**1**	**0.0**	**0.0**	**0.0**
	3	23.8	20.0	17.8
Th@C_s(15)-C_{84}	**1**	**0.0**	**0.0**	**0.0**
	3	16.4	12.6	10.5
Th@C_1(11)-C_{86}	**1**	**0.0**	**0.0**	**0.0**
	3	26.0	22.2	19.4
Th@C_2(14)-C_{86}	**1**	**0.0**	**0.0**	**0.0**
	3	17.1	13.7	11.8
Th@C_3(18)-C_{86}	**1**	**0.0**	**0.0**	**0.0**
	3	24.7	20.7	18.1
U@D_{3h}-C_{74}	**3**	**0.0**	**0.0**	**0.0**
	5	1.9	5.0	9.0
U@C_1(17418)-C_{76}	**3**	**0.0**	**0.0**	**0.0**
	5	2.7	1.8	7.1
U@C_1(28324)-C_{80}	**3**	**0.0**	**0.0**	**0.0**
	5	4.1	4.5	12.3
U@C_s(4)-C_{82}	**3**	**0.0**	**0.0**	**0.0**
	5	8.5	3.1	9.2
U@C_2(5)-C_{82}	**3**	**0.0**	**0.0**	**0.0**
	5	3.4	4.1	7.6
U@C_s(6)-C_{82}	**3**	**0.0**	**0.1**	**0.0**
	5	1.3	**0.0**	1.2
U@C_{2v}(9)-C_{82}	**3**	**0.0**	**0.2**	**0.0**
	5	3.3	**0.0**	2.8
U@C_2(8)-C_{84}	**3**	**0.0**	**0.0**	**0.0**
	5	2.1	7.1	12.1
U@C_s(15)-C_{84}	**3**	**0.0**	**0.0**	**0.0**
	5	5.3	6.3	11.3
U@D_2(21)-C_{84}	**3**	9.0	**0.0**	**0.0**
	5	**0.0**	0.5	4.1
U@C_1(11)-C_{86}	**3**	**0.1**	**0.0**	**0.0**
	5	**0.0**	7.2	11.7
U@C_1(12)-C_{86}	**3**	**0.0**	**0.0**	**0.0**

U@C_s(15)-C_{86}	5	6.0	5.0	8.1
	3	**0.0**	**0.0**	**0.0**
	5	3.0	1.9	9.1

Table S3 Computed and experimental first redox potentials (V *vs.* Fc/Fc^+) and electrochemical bandgaps of all 13 U-based mono-EMFs. The COSMO model was used to consider the solvent effect.

Species	Method (o-DCB)	$^{ox}E_1$	$^{red}E_1$	ΔE_{gap}	Ref.
U@D_{3h}-C_{74}	Exp.	0.01	-1.05	1.06	13
	M06-2X	-0.13	-0.81	0.68	this work
U@C_1(17418)-C_{76}	Exp.	0.14	-0.72	0.86	6
	M06-2X	0.17	-0.86	1.03	this work
U@C_1(28324)-C_{80}	Exp.	0.28	-0.57	0.85	6
	M06-2X	0.11	-0.86	0.97	this work
U@C_s(4)-C_{82}	Exp.	N/A	N/A	N/A	15
	M06-2X	-0.01	-0.95	0.94	this work
U@C_2(5)-C_{82}	Exp.	0.11	-0.67	0.78	13
	M06-2X	-0.09	-0.81	0.72	this work
U@C_s(6)-C_{82}	Exp.	0.04	-0.41	0.45	16
	M06-2X	0.16	-0.31	0.47	this work
U@C_{2v}(9)-C_{82}	Exp.	0.10	-0.43	0.53	13
	M06-2X	0.17	-0.69	0.86	this work
U@C_2(8)-C_{84}	Exp.	0.08	-0.75	0.83	16
	M06-2X	0.05	-0.98	1.03	this work
U@C_s(15)-C_{84}	Exp.	0.12	-0.71	0.83	16
	M06-2X	0.02	-0.57	0.59	this work
U@D_2(21)-C_{84}	Exp.	0.07	-0.68	0.75	17
	M06-2X	0.04	-0.60	0.64	this work
U@C_1(11)-C_{86}	Exp.	0.18	-0.69	0.87	17
	M06-2X	0.04	-0.59	0.63	this work
U@C_1(12)-C_{86}	Exp.	0.08	-0.78	0.86	16
	M06-2X	-0.02	-0.76	0.74	this work
U@C_s(15)-C_{86}	Exp.	0.24	-0.60	0.84	17
	M06-2X	0.29	-0.52	0.81	this work

Table S4 Encapsulation energies (E_e, kcal/mol) of all actinide mono-EMFs.

Species	E_e	Species	E_e
Th@T_d(2)-C_{76}	256.2	U@D_{3h}-C_{74}	151.5

Th@C_1(17418)-C_{76}	264.0	U@C_1(17418)-C_{76}	172.6
Th@D_{5h}(6)-C_{80}	257.5	U@C_1(28324)-C_{80}	177.6
Th@C_1(28324)-C_{80}	272.4	U@C_s(4)-C_{82}	140.5
Th@C_2(5)-C_{82}	231.3	U@C_2(5)-C_{82}	142.4
Th@C_{3v}(8)-C_{82}	270.1	U@C_s(6)-C_{82}	162.9
Th@C_{2v}(9)-C_{82}	255.5	U@C_{2v}(9)-C_{82}	176.7
Th@C_2(8)-C_{84}	239.5	U@C_2(8)-C_{84}	148.4
Th@C_s(15)-C_{84}	224.1	U@C_s(15)-C_{84}	133.7
Th@C_1(11)-C_{86}	239.4	U@D_2(21)-C_{84}	150.5
Th@C_2(14)-C_{86}	248.2	U@C_1(11)-C_{86}	144.8
Th@C_3(18)-C_{86}	236.3	U@C_1(12)-C_{86}	147.0
		U@C_s(15)-C_{86}	151.1

Table S5 Calculated metal charges (CM5) of all actinide mono-EMFs at different theoretical levels.

Species	M06-2X	PBE0	PBE	Species	M06-2X	PBE0	PBE
Th@T_d(2)-C_{76}	+1.61	+1.56	+1.44	U@D_{3h}-C_{74}	+1.29	+1.33	+1.26
Th@C_1(17418)-C_{76}	+1.61	+1.56	+1.45	U@C_1(17418)-C_{76}	+1.29	+1.33	+1.29
Th@D_{5h}(6)-C_{80}	+1.63	+1.57	+1.46	U@C_1(28324)-C_{80}	+1.46	+1.41	+1.30
Th@C_1(28324)-C_{80}	+1.60	+1.55	+1.44	U@C_s(4)-C_{82}	+1.33	+1.40	+1.28
Th@C_2(5)-C_{82}	+1.60	+1.55	+1.43	U@C_2(5)-C_{82}	+1.30	+1.31	+1.28
Th@C_{3v}(8)-C_{82}	+1.60	+1.55	+1.44	U@C_s(6)-C_{82}	+1.24	+1.21	+1.20
Th@C_{2v}(9)-C_{82}	+1.59	+1.54	+1.42	U@C_{2v}(9)-C_{82}	+1.24	+1.22	+1.22
Th@C_2(8)-C_{84}	+1.59	+1.54	+1.42	U@C_2(8)-C_{84}	+1.29	+1.33	+1.27
Th@C_s(15)-C_{84}	+1.58	+1.53	+1.42	U@C_s(15)-C_{84}	+1.32	+1.34	+1.27
Th@C_1(11)-C_{86}	+1.59	+1.54	+1.43	U@D_2(21)-C_{84}	+1.23	+1.23	+1.23
Th@C_2(14)-C_{86}	+1.60	+1.55	+1.43	U@C_1(11)-C_{86}	+1.43	+1.35	+1.26
Th@C_3(18)-C_{86}	+1.59	+1.54	+1.42	U@C_1(12)-C_{86}	+1.27	+1.29	+1.27
				U@C_s(15)-C_{86}	+1.26	+1.25	+1.23

Table S6 Spin population values of all U-based mono-EMFs.

Species	Spin population
U@D_{3h}-C_{74}	3.00
U@C_1(17418)-C_{76}	3.02

U@C_1(28324)-C_{80}	2.44
U@C_s(4)-C_{82}	2.88
U@C_2(5)-C_{82}	2.99
U@C_s(6)-C_{82}	3.14
U@C_{2v}(9)-C_{82}	3.14
U@C_2(8)-C_{84}	2.99
U@C_s(15)-C_{84}	2.92
U@D_2(21)-C_{84}	3.17
U@C_1(11)-C_{86}	3.15
U@C_1(12)-C_{86}	3.05
U@C_s(15)-C_{86}	3.05

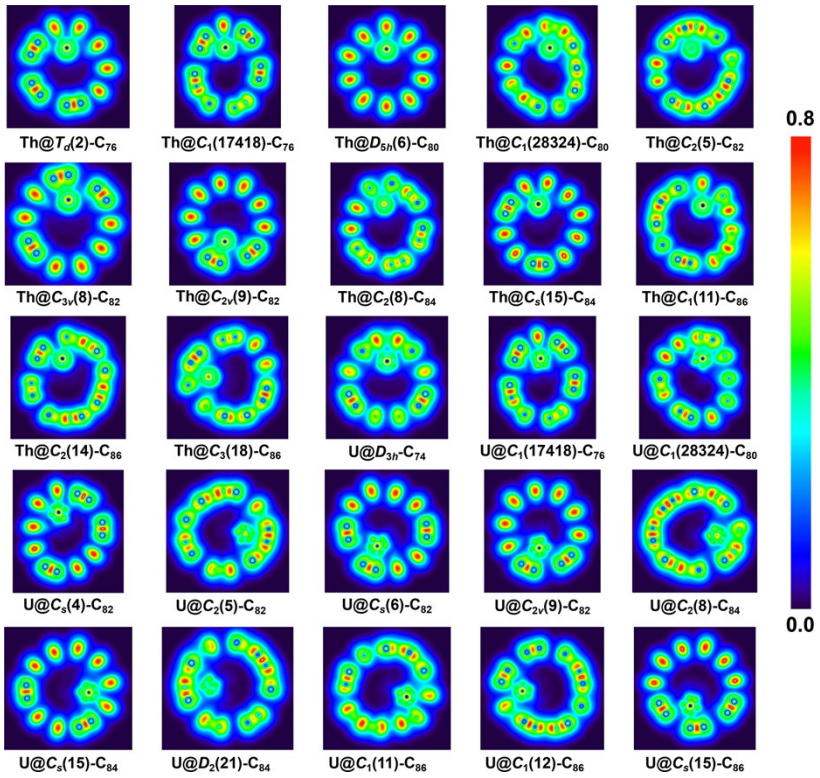

Fig. S1 LOL plots on a plane containing metal atom for all actinide mono-EMFs.

Table S7 IQA interaction energy (V_{Int}, kcal/mol), coulombic energy (V_C, kcal/mol), and interatomic exchange-correlation (V_{XC}, kcal/mol) components between metal and the nearest neighbor carbon atoms in actinide mono-EMFs.

Species	V_{Int}**(M,C)**	V_C**(M,C)**	V_{XC}**(M,C)**	**Species**	V_{Int}**(M,C)**	V_C**(M,C)**	V_{XC}**(M,C)**
Th@T_d(2)-C_{76}	-86.0	-48.4	-37.6	U@D_{3h}-C_{74}	-75.8	-39.7	-36.1

Th@C_1(17418)-C_{76}	-79.9	-44.2	-35.7	U@C_1(17418)-C_{76}	-64.6	-31.8	-32.8
Th@D_{5h}-C_{80}	-97.3	-51.5	-45.8	U@C_1(28324)-C_{80}	-80.2	-37.2	-43.0
Th@C_1(28324)-C_{80}	-87.1	-49.2	-37.9	U@C_s(4)-C_{82}	-72.6	-34.8	-37.8
Th@C_2(5)-C_{82}	-87.9	-47.7	-40.2	U@C_2(5)-C_{82}	-72.0	-35.2	-36.8
Th@C_{3v}(8)-C_{82}	-90.9	-43.6	-47.3	U@C_s(6)-C_{82}	-67.8	-28.0	-39.8
Th@C_{2v}(9)-C_{82}	-94.8	-45.9	-48.9	U@C_{2v}(9)-C_{82}	-74.2	-41.3	-32.9
Th@C_2(8)-C_{84}	-96.5	-53.8	-42.7	U@C_2(8)-C_{84}	-79.0	-39.5	-39.5
Th@C_s(15)-C_{84}	-92.7	-51.2	-41.4	U@C_s(15)-C_{84}	-77.1	-36.9	-40.2
Th@C_1(11)-C_{86}	-86.5	-47.5	-39.0	U@D_2(21)-C_{84}	-75.0	-35.8	-39.2
Th@C_2(14)-C_{86}	-86.9	-48.1	-38.8	U@C_1(11)-C_{86}	-75.5	-34.3	-41.2
Th@C_3(18)-C_{86}	-95.8	-53.2	-42.6	U@C_1(12)-C_{86}	-69.3	-34.8	-34.6
				U@C_s(15)-C_{86}	-79.0	-37.3	-41.7

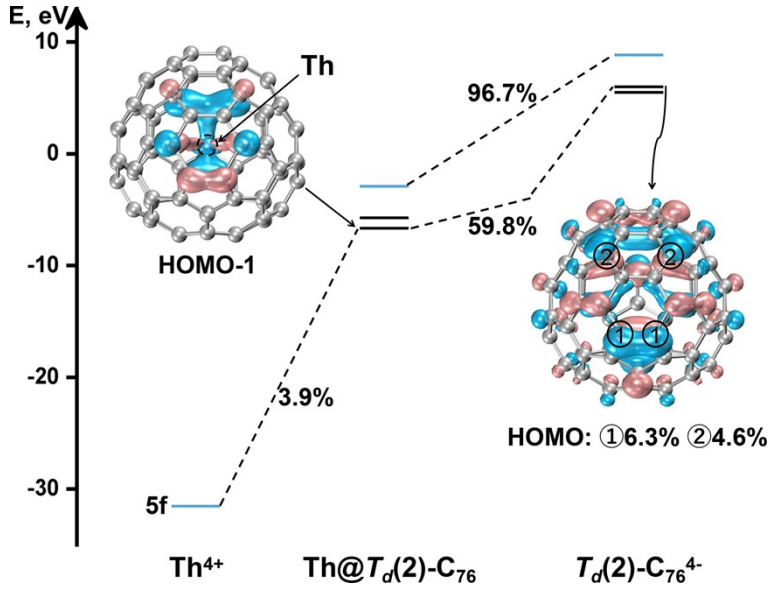

Fig. S2 Orbital interaction diagrams based on metal cation and cage anion of

Th@T_d(2)-C_{76}. For clarity, only the occupied molecular orbitals with significant overlaps between metal and cage are shown.

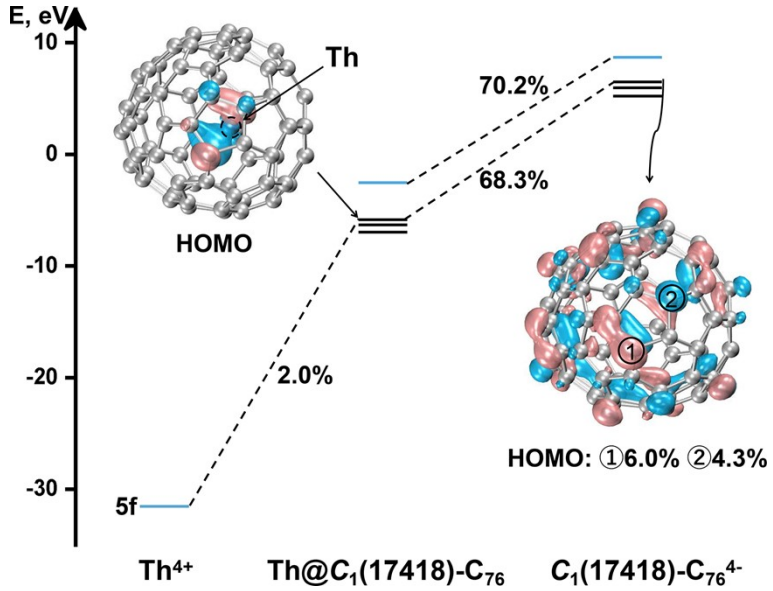

Fig. S3 Orbital interaction diagrams based on metal cation and cage anion of Th@C_1(17418)-C_{76}. For clarity, only the occupied molecular orbitals with significant overlaps between metal and cage are shown.

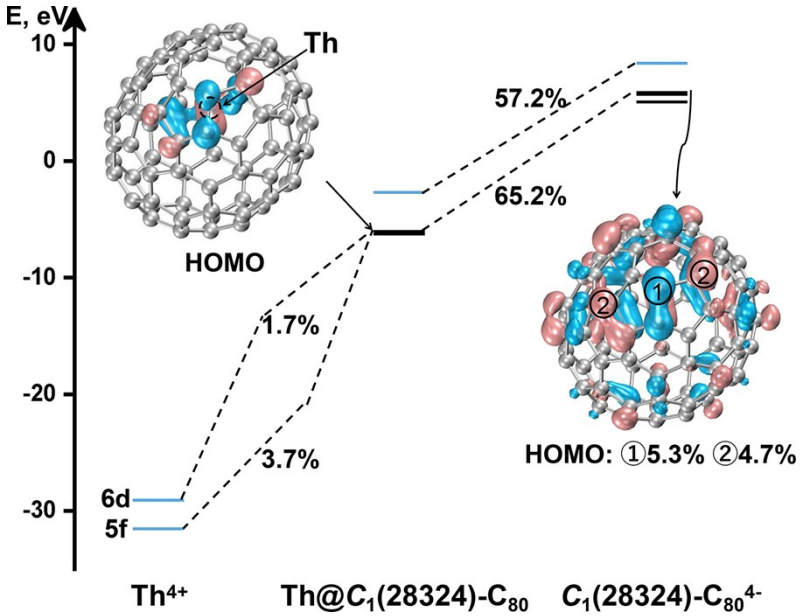

Fig. S4 Orbital interaction diagrams based on metal cation and cage anion of Th@C_1(28324)-C_{80}. For clarity, only the occupied molecular orbitals with significant overlaps between metal and cage are shown.

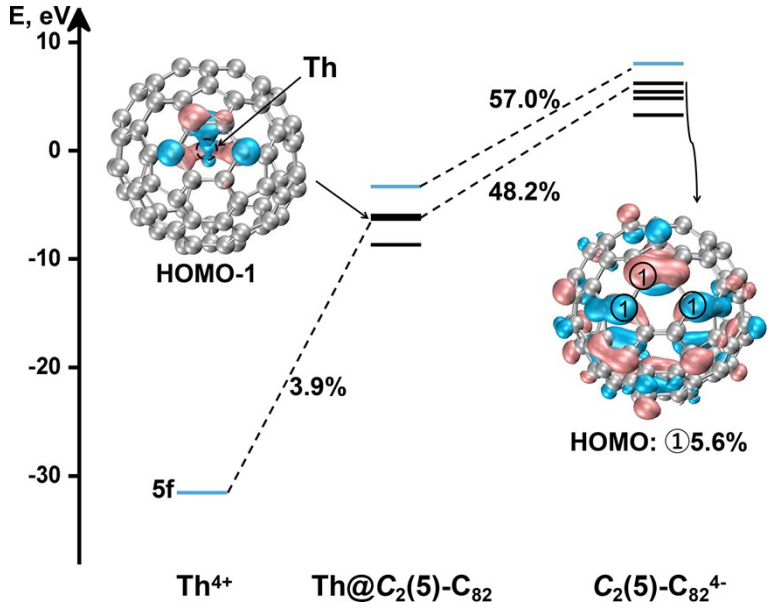

Fig. S5 Orbital interaction diagrams based on metal cation and cage anion of Th@C_2(5)-C_{82}. For clarity, only the occupied molecular orbitals with significant overlaps between metal and cage are shown.

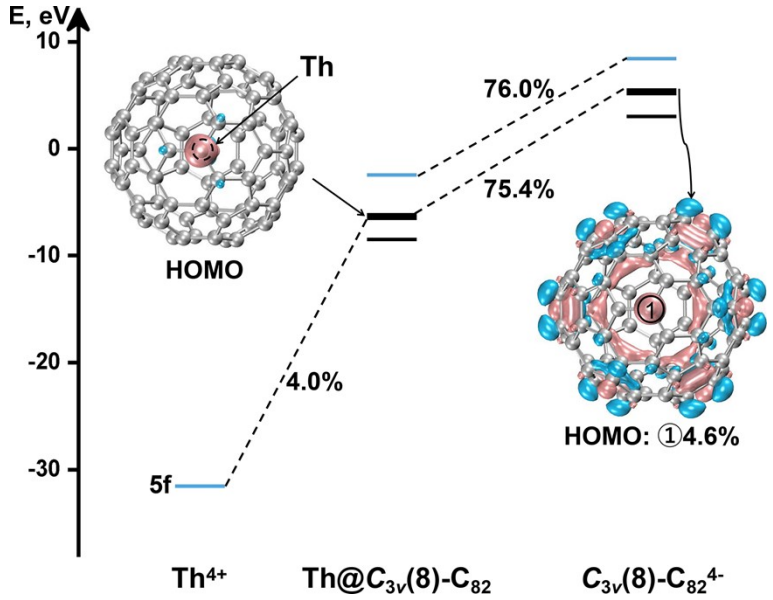

Fig. S6 Orbital interaction diagrams based on metal cation and cage anion of Th@C_{3v}(8)-C_{82}. For clarity, only the occupied molecular orbitals with significant

overlaps between metal and cage are shown.

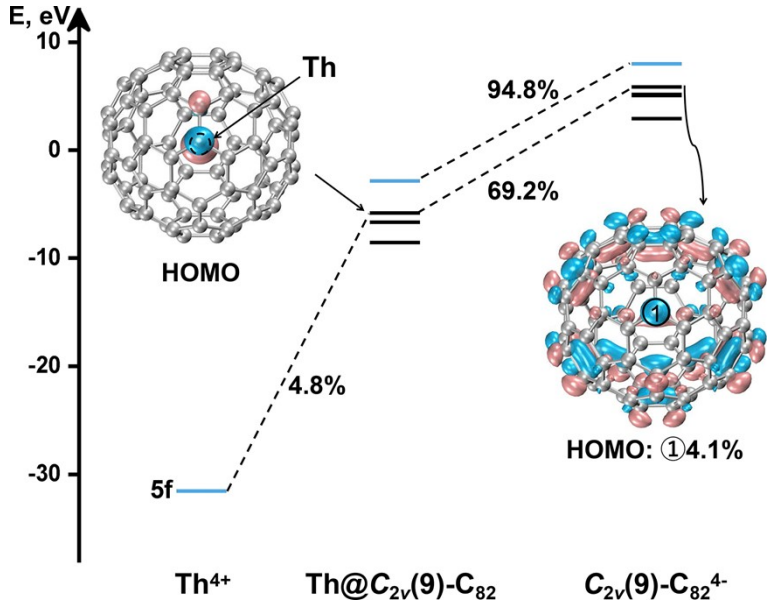

Fig. S7 Orbital interaction diagrams based on metal cation and cage anion of Th@C_{2v}(9)-C_{82}. For clarity, only the occupied molecular orbitals with significant overlaps between metal and cage are shown.

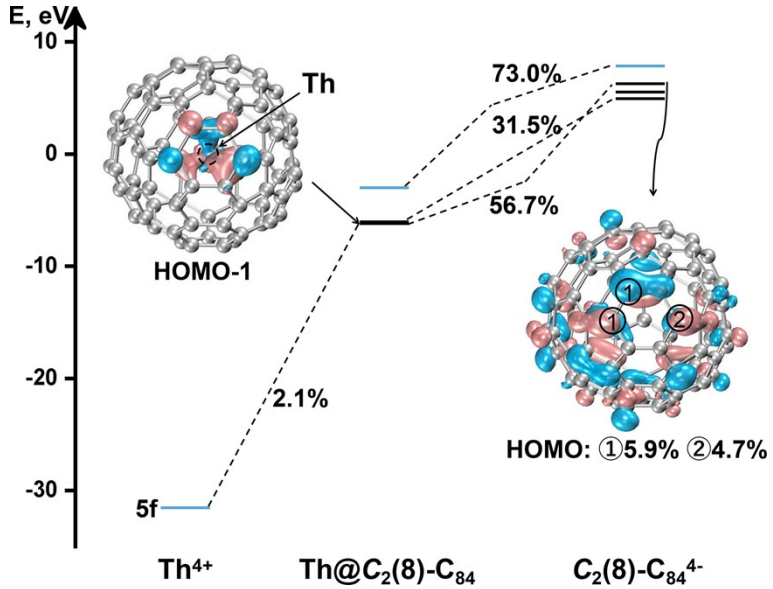

Fig. S8 Orbital interaction diagrams based on metal cation and cage anion of Th@C_2(8)-C_{84}. For clarity, only the occupied molecular orbitals with significant overlaps between metal and cage are shown.

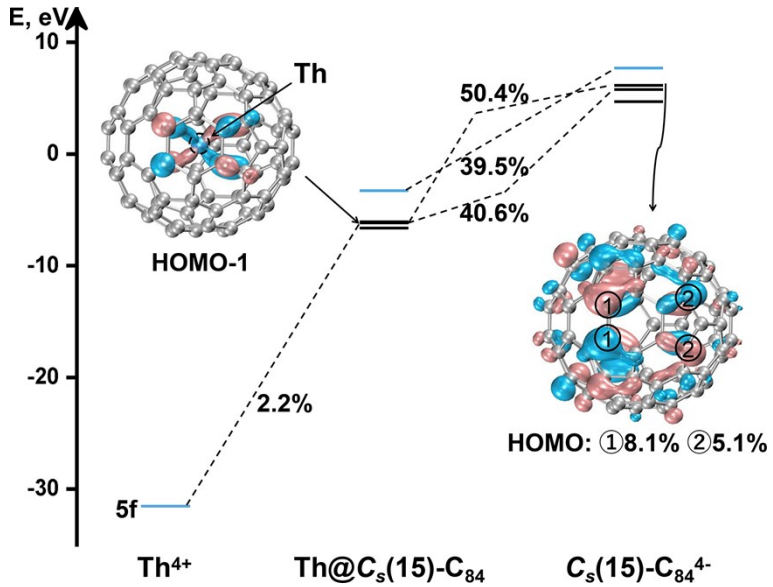

Fig. S9 Orbital interaction diagrams based on metal cation and cage anion of Th@C_s(15)-C_{84}. For clarity, only the occupied molecular orbitals with significant overlaps between metal and cage are shown.

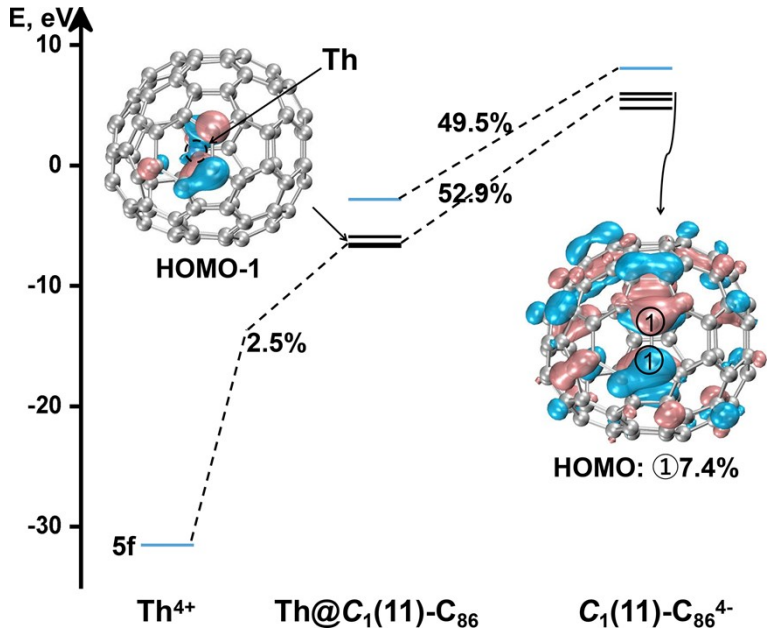

Fig. S10 Orbital interaction diagrams based on metal cation and cage anion of

Th@C_1(11)-C_{86}. For clarity, only the occupied molecular orbitals with significant overlaps between metal and cage are shown.

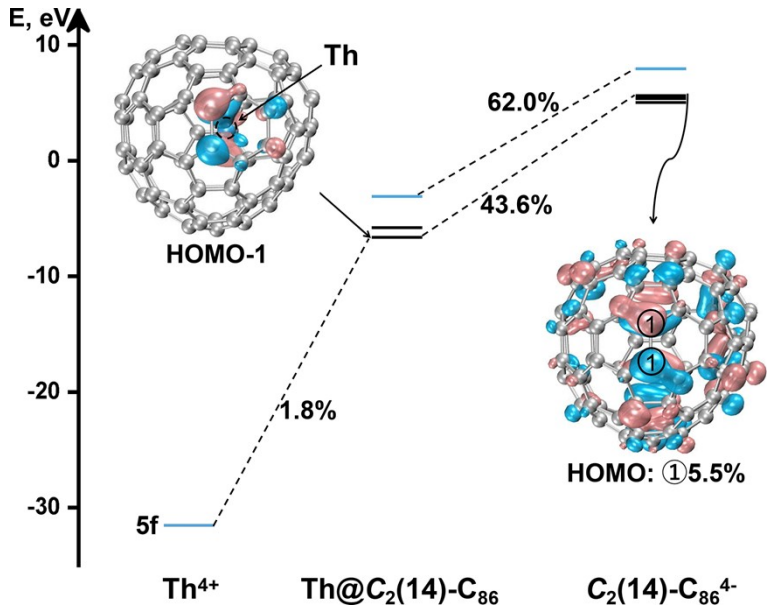

Fig. S11 Orbital interaction diagrams based on metal cation and cage anion of Th@C_2(14)-C_{86}. For clarity, only the occupied molecular orbitals with significant overlaps between metal and cage are shown.

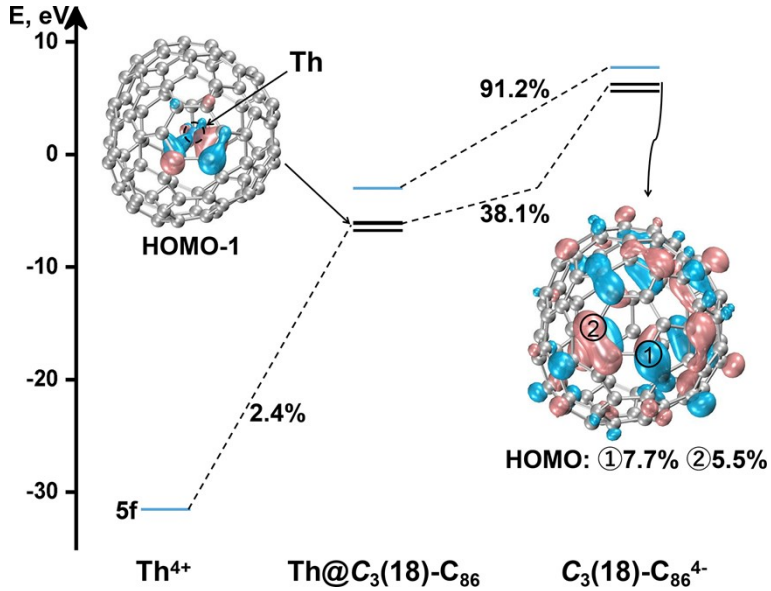

Fig. S12 Orbital interaction diagrams based on metal cation and cage anion of Th@C_3(18)-C_{86}. For clarity, only the occupied molecular orbitals with significant

overlaps between metal and cage are shown.

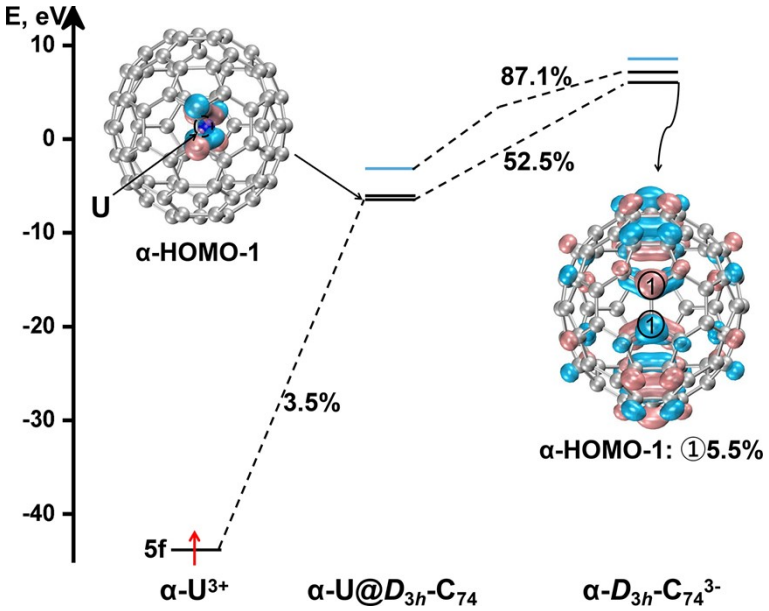

Fig. S13 Orbital interaction diagrams based on metal cation and cage anion of U@D_{3h}-C_{74}. For clarity, only the occupied molecular orbitals with significant overlaps between metal and cage are shown with other orbitals and electrons omitted.

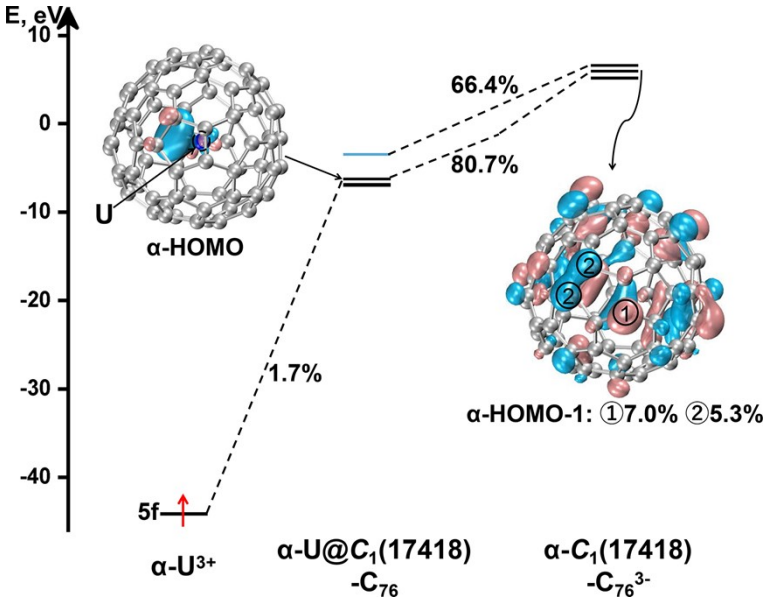

Fig. S14 Orbital interaction diagrams based on metal cation and cage anion of U@C_1(17418)-C_{76}. For clarity, only the occupied molecular orbitals with significant

overlaps between metal and cage are shown with other orbitals and electrons omitted.

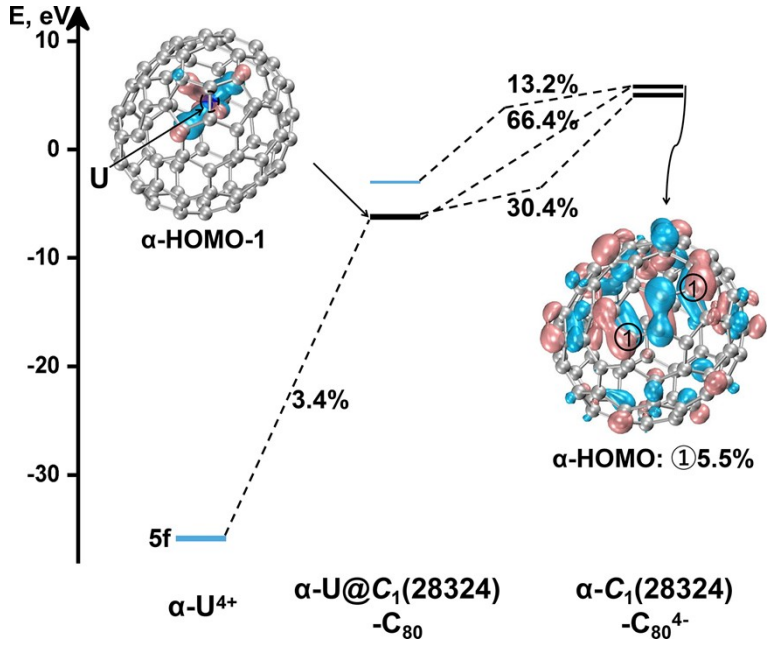

Fig. S15 Orbital interaction diagrams based on metal cation and cage anion of U@C_1(28324)-C_{80}. For clarity, only the occupied molecular orbitals with significant overlaps between metal and cage are shown with other orbitals and electrons omitted.

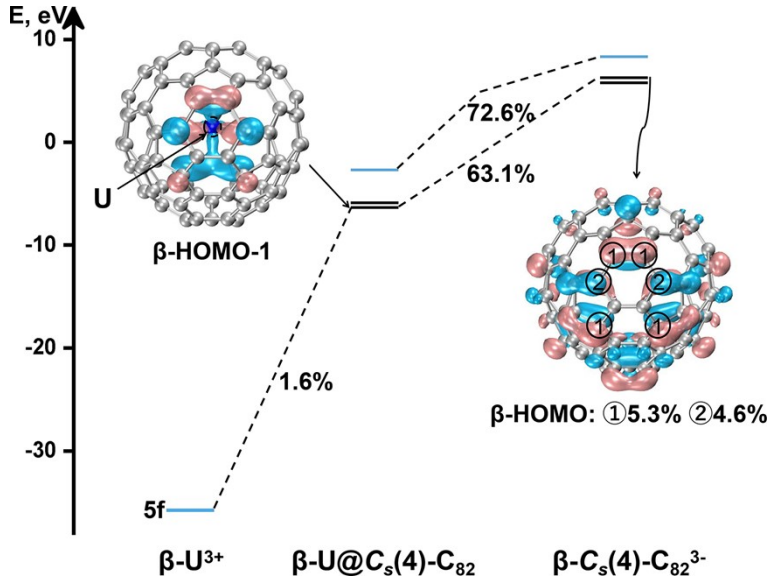

Fig. S16 Orbital interaction diagrams based on metal cation and cage anion of

U@C_s(4)-C_{82}. For clarity, only the occupied molecular orbitals with significant overlaps between metal and cage are shown with other orbitals and electrons omitted.

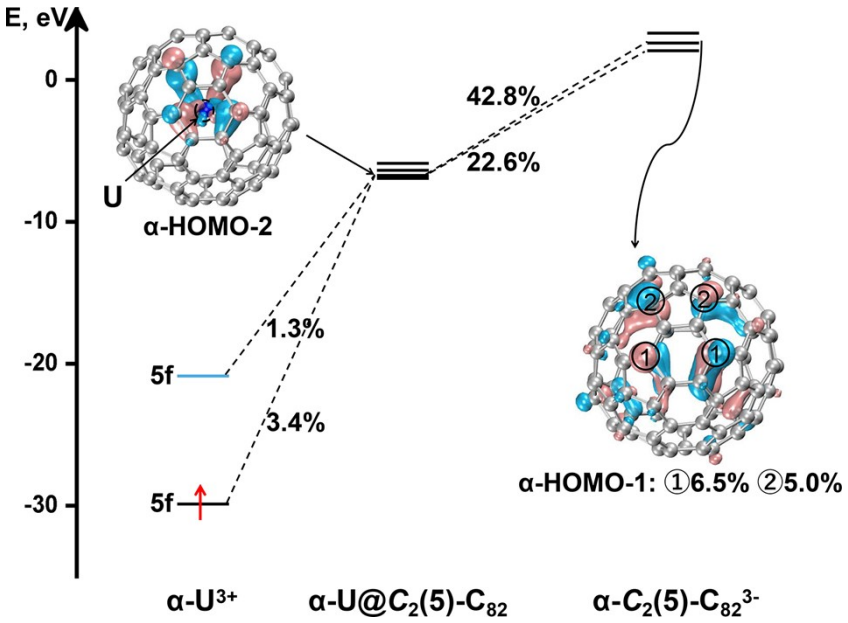

Fig. S17 Orbital interaction diagrams based on metal cation and cage anion of U@C_2(5)-C_{82}. For clarity, only the occupied molecular orbitals with significant overlaps between metal and cage are shown with other orbitals and electrons omitted.

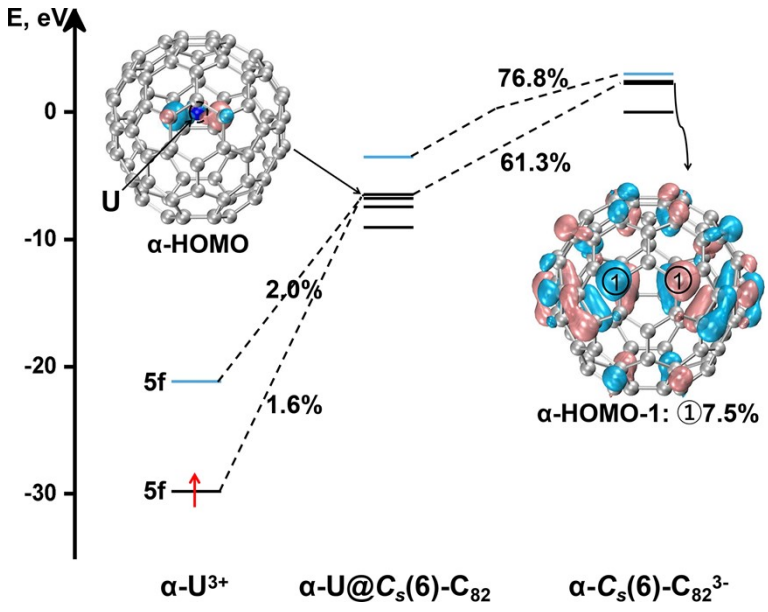

Fig. S18 Orbital interaction diagrams based on metal cation and cage anion of U@C_s(6)-C_{82}. For clarity, only the occupied molecular orbitals with significant overlaps between metal and cage are shown with other orbitals and electrons omitted.

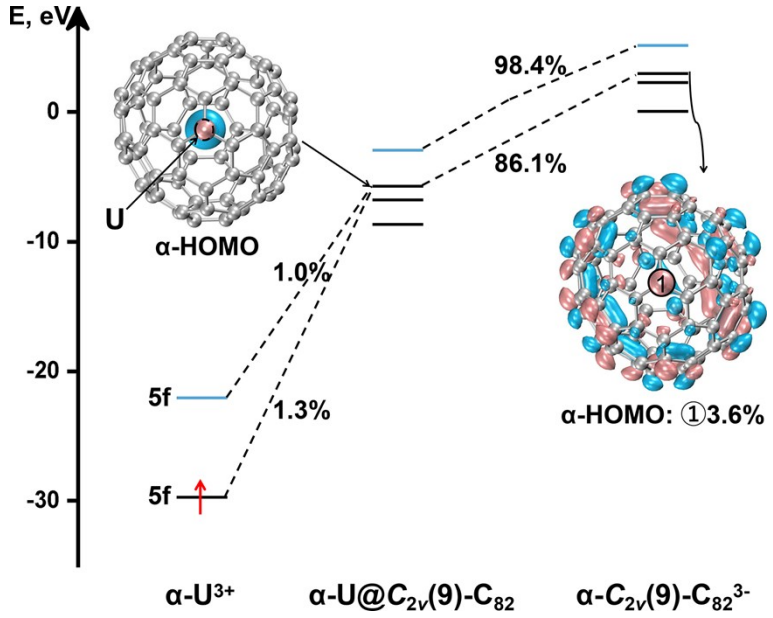

Fig. S19 Orbital interaction diagrams based on metal cation and cage anion of U@C_{2v}(9)-C_{82}. For clarity, only the occupied molecular orbitals with significant overlaps between metal and cage are shown with other orbitals and electrons omitted.

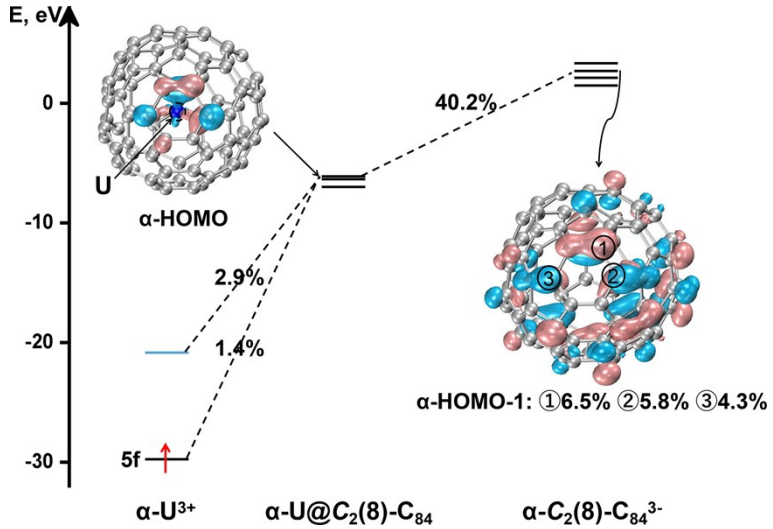

Fig. S20 Orbital interaction diagrams based on metal cation and cage anion of U@C_2(8)-C_{84}. For clarity, only the occupied molecular orbitals with significant

overlaps between metal and cage are shown with other orbitals and electrons omitted.

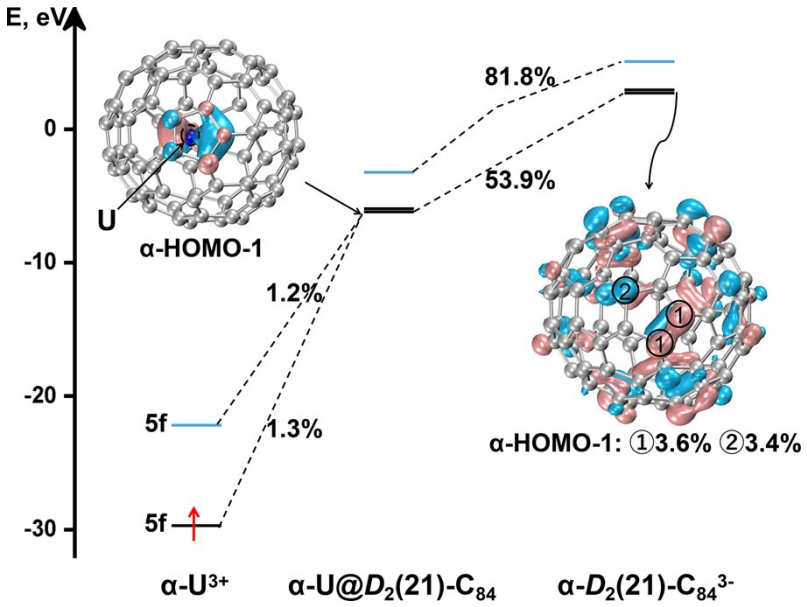

Fig. S21 Orbital interaction diagrams based on metal cation and cage anion of U@D_2(21)-C_{84}. For clarity, only the occupied molecular orbitals with significant overlaps between metal and cage are shown with other orbitals and electrons omitted.

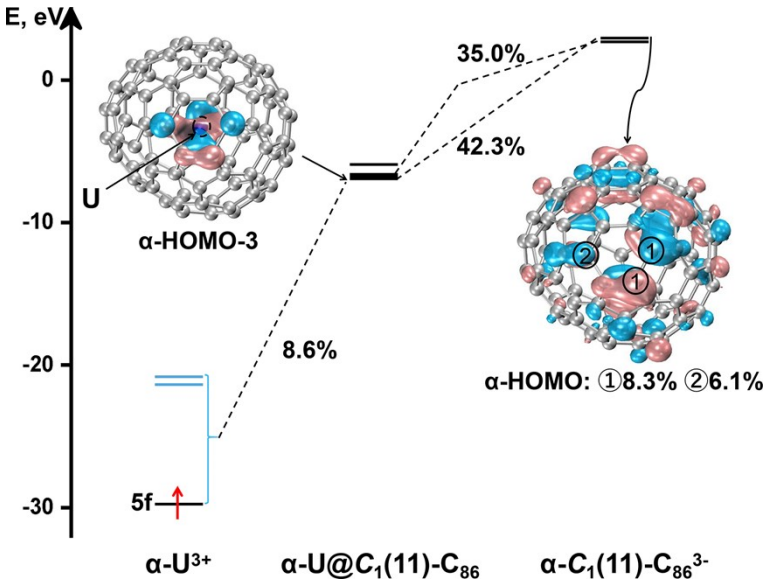

Fig. S22 Orbital interaction diagrams based on metal cation and cage anion of U@C_1(11)-C_{86}. For clarity, only the occupied molecular orbitals with significant overlaps between metal and cage are shown with other orbitals and electrons omitted.

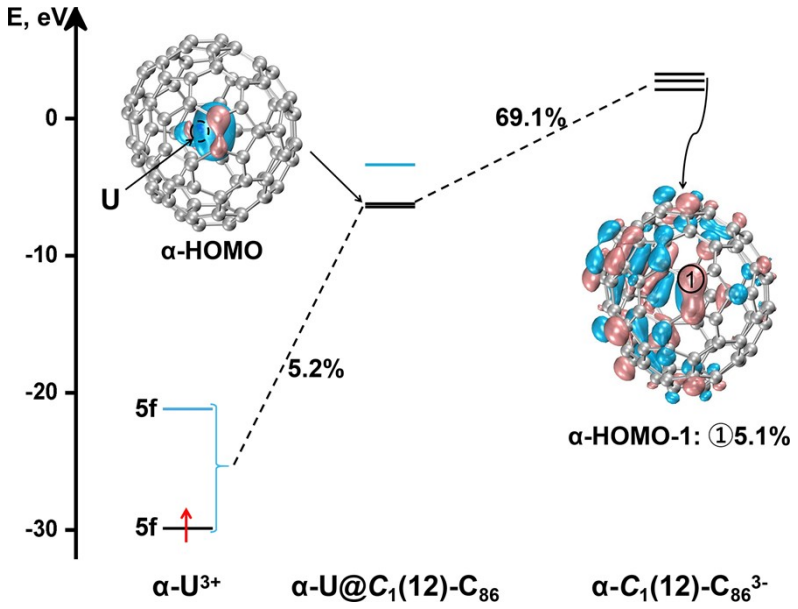

Fig. S23 Orbital interaction diagrams based on metal cation and cage anion of U@C_1(12)-C_{86}. For clarity, only the occupied molecular orbitals with significant overlaps between metal and cage are shown with other orbitals and electrons omitted.

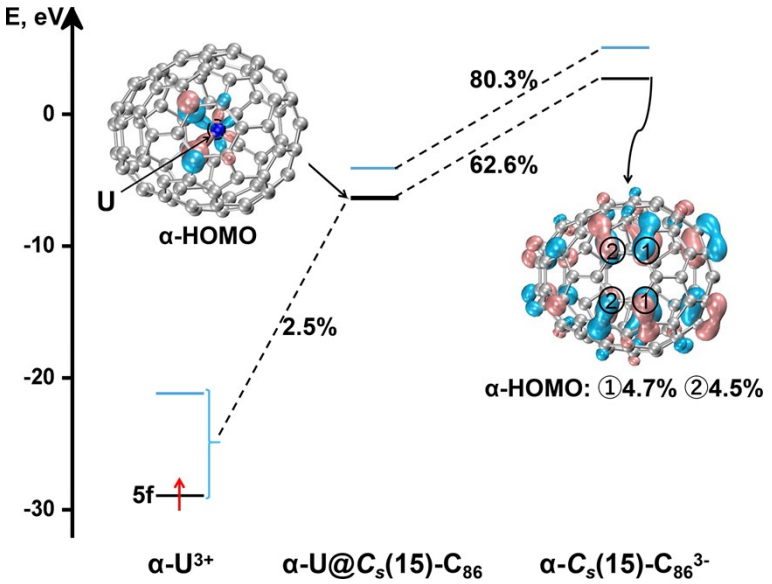

Fig. S24 Orbital interaction diagrams based on metal cation and cage anion of U@C_s(15)-C_{86}. For clarity, only the occupied molecular orbitals with significant overlaps between metal and cage are shown with other orbitals and electrons omitted.

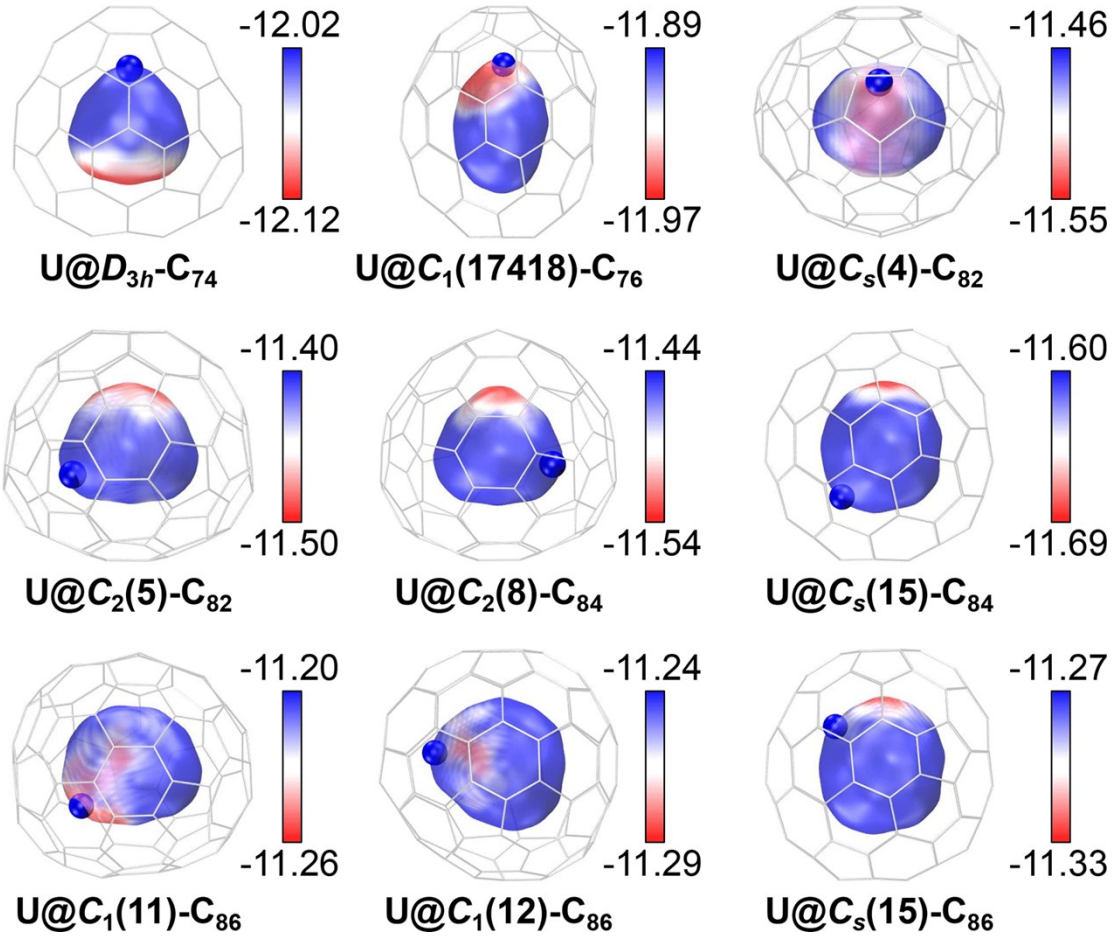

Fig. S25 The overlaps of the structures of nine U-based mono-EMFs with the ESP isosurfaces (eV) inside the corresponding C_{2n}^{4-} empty cages (PBE level).

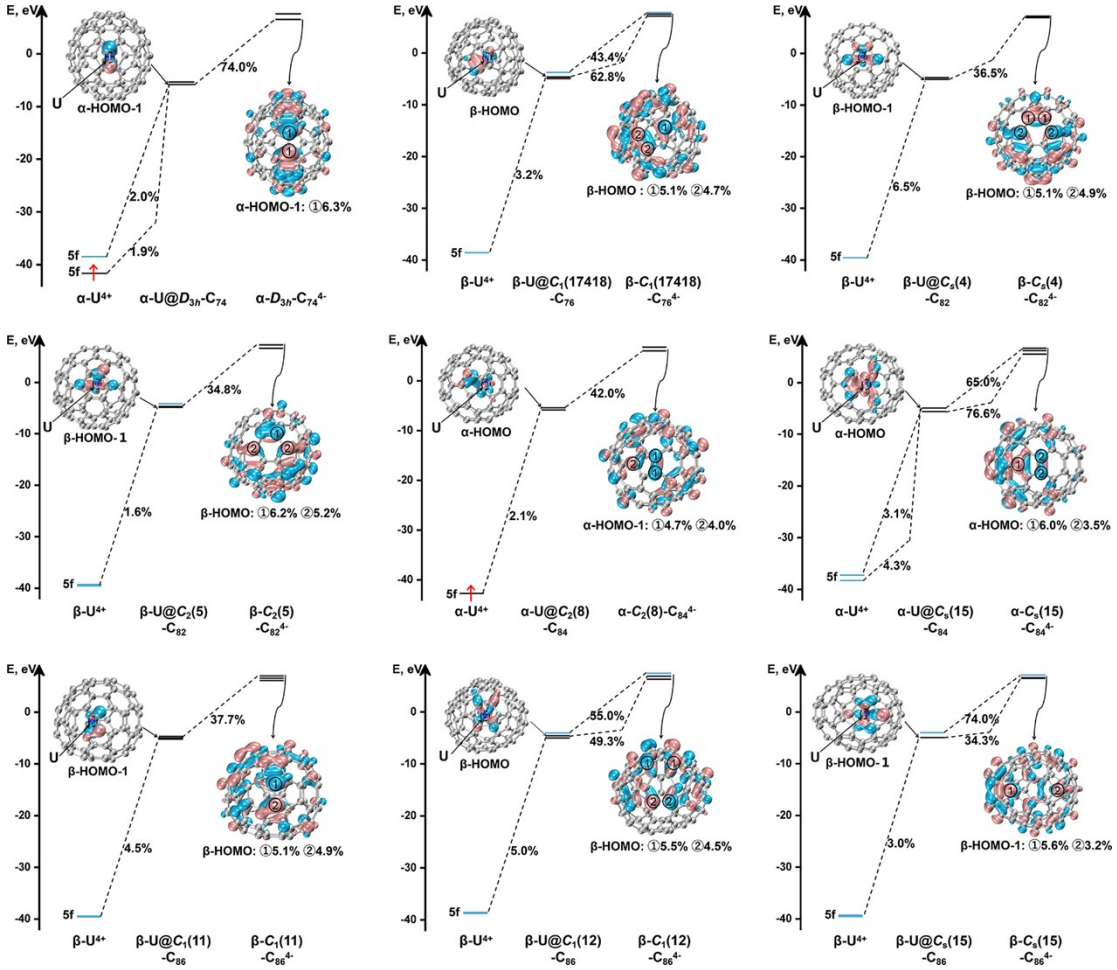

Fig. S26 Orbital interaction diagrams based on metal cation and cage anion of nine U-based mono-EMFs (PBE level). For clarity, only the occupied molecular orbitals with significant overlaps between metal and cage are shown with other orbitals and electrons omitted.

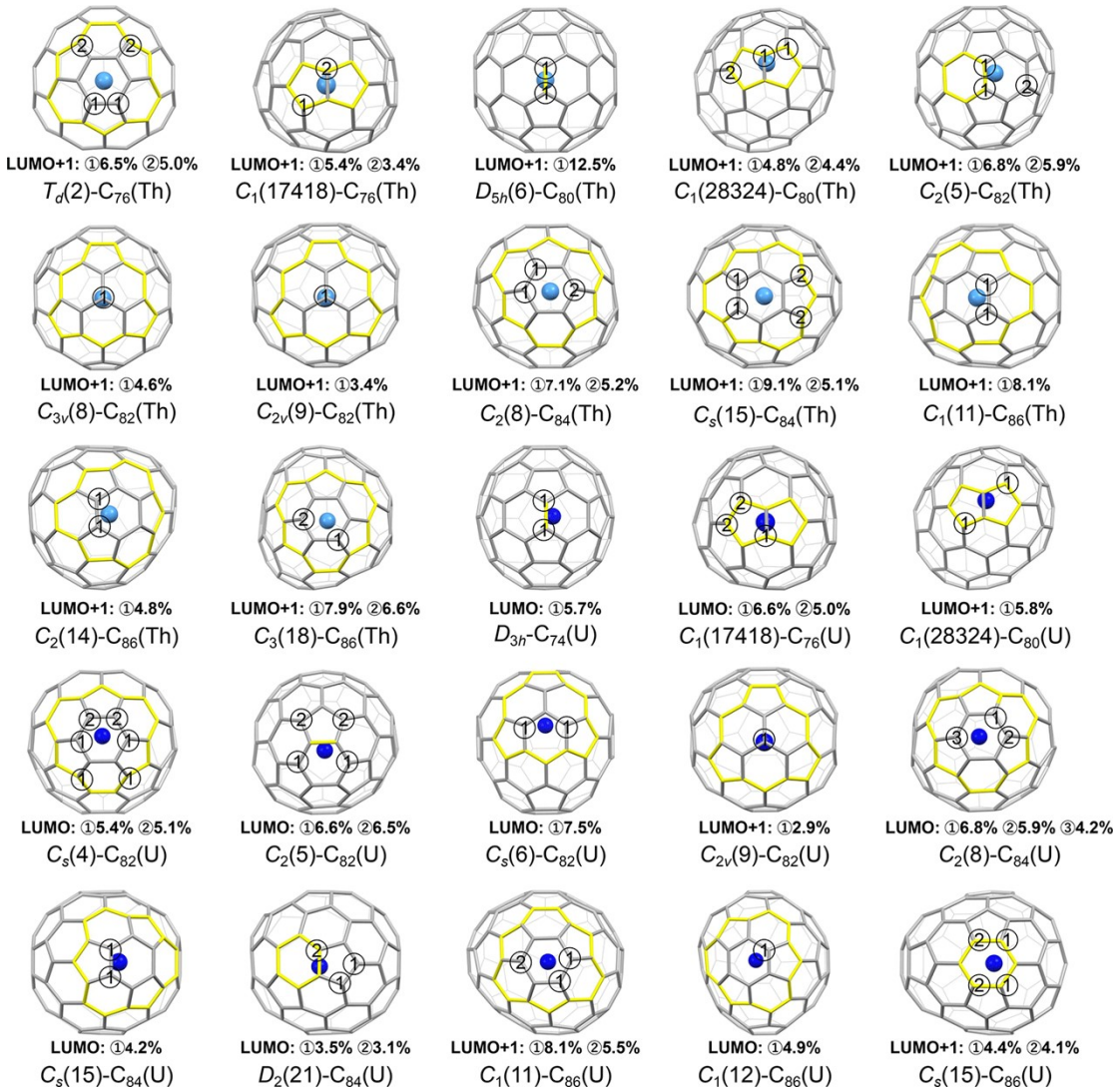

Fig. S27 Overlaps between the structures of all actinide mono-EMFs and the orbital composition analyses of corresponding neutral hollow cages. The carbon atoms that contribute (in %) most to the corresponding orbitals are numbered. The cage segments interacting with the metals in the single crystal structures are circled by yellow. Th: light blue; U: dark blue.

References

1 M. Jin, J. Zhuang, Y. Wang, W. Yang, X. Liu and N. Chen, Th@T_d(19151)-C_{76}: a highly symmetric fullerene cage stabilized by a tetravalent actinide metal ion, *Inorg. Chem.*, 2019, **58**, 16722-16726.

2 P. Jin, C. Liu, Y. Li, L. Li and Y. Zhao, Th@C_{76}. Computational characterization of larger

actinide endohedral fullerenes, *Int. J. Quantum Chem.*, 2018, **118**, e25501.

3 P. Zhao, X. Zhao and M. Ehara, Theoretical insights into monometallofullerene Th@C_{76}: strong covalent interaction between thorium and the carbon cage, *Inorg. Chem.*, 2018, **57**, 2961-2964.

4 Y. Xia, Y. Shen, Y.-R. Yao, Q. Meng and N. Chen, Synthesis and characterization of a novel non-isolated-pentagon-rule isomer of Th@C_{76}: Th@C_1(17418)-C_{76}, *Inorganics*, 2023, **11**, 422.

5 Y. Yan, R. Morales-Martínez, J. Zhuang, Y.-R. Yao, X. Li, J. M. Poblet, A. Rodríguez-Fortea and N. Chen, Th@D_{5h}(6)-C_{80}: a highly symmetric fullerene cage stabilized by a single metal ion, *Chem. Commun.*, 2021, **57**, 6624-6627.

6 W. Cai, L. Abella, J. Zhuang, X. Zhang, L. Feng, Y. Wang, R. Morales-Martínez, R. Esper, M. Boero, A. Metta-Magaña, A. Rodríguez-Fortea, J. M. Poblet, L. Echegoyen and N. Chen, Synthesis and characterization of non-isolated-pentagon-rule actinide endohedral metallofullerenes U@C_1(17418)-C_{76}, U@C_1(28324)-C_{80}, and Th@C_1(28324)-C_{80}: low-symmetry cage selection directed by a tetravalent ion, *J. Am. Chem. Soc.*, 2018, **140**, 18039-8050.

7 Q. Meng, R. Morales-Martínez, J. Zhuang, Y.-R. Yao, Y. Wang, L. Feng, J. M. Poblet, A. Rodríguez-Fortea and N. Chen, Synthesis and characterization of two isomers of Th@C_{82}: Th@C_{2v}(9)-C_{82} and Th@C_2(5)-C_{82}, *Inorg. Chem.*, 2021, **60**, 11496-11502.

8 Y. Wang, R. Morales-Martínez, X. Zhang, W. Yang, Y. Wang, A. Rodríguez-Fortea, J. M. Poblet, L. Feng, S. Wang and N. Chen, Unique four-electron metal-to-cage charge transfer of Th to a C_{82} fullerene cage: complete structural characterization of Th@C_{3v}(8)-C_{82}, *J. Am. Chem. Soc.*, 2017, **139**, 5110-5116.

9 X. Liu, B. Li, W. Yang, Y.-R. Yao, L. Yang, J. Zhuang, X. Li, P. Jin and N. Chen, Synthesis and characterization of carbene derivatives of Th@C_{3v}(8)-C_{82} and U@C_{2v}(9)-C_{82}: exceptional chemical properties induced by strong actinide-carbon cage interaction, *Chem. Sci.*, 2020, **12**, 2488-2497.

10 T. Cao, Q. Meng, Z. Fu, Y. Shen, Y. Yan, Q. Wang, B. Zhao, W. Wang, K. Merimi, A. Rodríguez-Fortea, Y-R. Yao and N. Chen, Th@C_2(8)-C_{84} and Th@C_s(15)-C_{84}: impact of actinide metal ions on the electronic structures of actinide endohedral metallofullerenes, *Inorg. Chem. Front.*, 2023, **10**, 6901-6908.

11 Y. Wang, R. Morales-Martínez, W. Cai, J. Zhuang, W. Yang, L. Echegoyen, J. M. Poblet, A. Rodríguez-Fortea and N. Chen, Th@C_1(11)-C_{86}: an actinide encapsulated in an unexpected C_{86} fullerene cage, *Chem. Commun.*, 2019, **55**, 9271-9274.

12 J. Qiu, L. Zheng, Y. Roselló, K. Merimi, Y.-R. Yao, Z. Cao, Z. He, J M. Poblet, A. Rodríguez-Fortea and N. Chen, Th@C_2(14)-C_{86} and Th@C_3(18)-C_{86}: two missing C_{86} isomers stabilized by the encapsulation of thorium, *Inorg. Chem. Front.*, 2024, **11**, 3578-3584.

13 W. Cai, R. Morales-Martínez, X. Zhang, D. Najera, E. L. Romero, A. Metta-Magaña, A. Rodríguez-Fortea, S. Fortier, N. Chen, J. M. Poblet and L. Echegoyen, Single crystal structures and theoretical calculations of uranium endohedral metallofullerenes (U@C_{2n}, $2n$ = 74, 82)

show cage isomer dependent oxidation states for U, *Chem. Sci.*, 2017, **8**, 5282-5290.

14 Y.-X. Gu, Q.-Z. Li, P. Zhao and X. Zhao, Encapsulation of monometal uranium into fullerenes C_{2n} ($2n$ = 70−74): Important ionic $U^{4+}C_{2n}^{4-}$ characters and covalent U-cage bonding interactions, *Inorg. Chem.*, 2019, **58**, 10629-10636.

15 Q. Wang, L. Abella, Y-R. Yao, Y. Yan, D. Torrens, Q. Meng, S. Yang, J M. Poblet, A. Rodríguez-Fortea and N. Chen, U@C_s(4)-C_{82}: a different cage isomer with reactivity controlled by U-sumanene interaction, *Inorg. Chem.*, 2023, **62**, 12976-12988.

16 Y.-R. Yao, Y. Roselló, L. Ma, A. R. Puente Santiago, A. Metta-Magaña, N. Chen, A. Rodríguez-Fortea, J. M. Poblet and L. Echegoyen, Crystallographic characterization of U@C_{2n} ($2n$ = 82-86): insights about metal-cage interactions for mono-metallofullerenes, *J. Am. Chem. Soc.*, 2021, **143**, 15309-15318.

17 W. Cai, J. Alvarado, A. Metta-Magaña, N. Chen and L. Echegoyen, Interconversions between uranium mono-metallofullerenes: mechanistic implications and role of asymmetric cages, *J. Am. Chem. Soc.*, 2020, **142**, 13112-13119.